Nuclear Engineering and Technology 57 (2025) 103310

Contents lists available at ScienceDirect

Nuclear Engineering and Technology

journal homepage: www.elsevier.com/locate/net

Original Article

Comparison of UV-enhanced SiPM technologies for estimating 511 keV photon arrival time using BGO Cherenkov Luminescence

Andrea Gonzalez-Montoro [a,e], Shirin Pourashraf [a], Stefano Merzi [f], Alberto Gola [f], Craig S. Levin [a,b,c,d,*]

[a] Department of Radiology, Molecular Imaging Program at Stanford University, Stanford, CA 94305, United States
[b] Department of Physics, Stanford University, California, United States
[c] Department of Electrical Engineering, Stanford University, California, United States
[d] Department of Bioengineering, Stanford University, California, United States
[e] Instituto de Instrumentación para Imagen Molecular (i3M), Centro Mixto CSIC - Universitat Politècnica de València, Camino de Vera s/n, 46022 Valencia, Spain
[f] Fondazione Bruno Kessler, Trento, Italy

ARTICLE INFO

Keywords:
Positron emission tomography1
Time-of-flight2
BGO_3
Cherenkov radiation4
UV SiPMs5

ABSTRACT

Time-of-flight (TOF) is a method to boost reconstructed image signal-to-noise ratio in positron emission tomography (PET); the SNR gain increases as detector coincidence time resolution (CTR) improves. It is also desirable to control detector costs, especially when developing long axial field of view PET systems. With these two goals in mind, it has been proposed to exploit the prompt luminescence, predominantly Cherenkov light, in the scintillation crystal BGO, to estimate the annihilation photon arrival time for PET detectors. However, properly identifying the relatively low number of Cherenkov photons generated per interaction event in BGO is not easy, requires low noise photodetectors, fast readout electronics, and accurate signal processing techniques. Since Cherenkov photons are produced in the ultra-violet (UV) realm, photosensor technology with enhanced performance in the UV region is essential for best performance. In this work we have evaluated and compared the performance of three different UV-enhanced silicon photomultiplier (SiPMs) coupled to 3×3 mm^2 BGO scintillators ranging from 3 mm to 15 mm length, and two different readout circuits. State-of-the-art data post-processing methods have been employed for CTR estimation, consistently yielding CTR values < 300 ps full-width-at-half-maximum (FWHM) for all crystal lengths studied. To our knowledge, this is the first work comparing these UV-SiPM models under the same conditions.

1. Introduction

Efforts towards effectively increasing the already high sensitivity of positron emission tomography (PET) scanners have been pursued during the last years [1,2]. Sensitivity gains can be accomplished either by extending the axial coverage of the scanners (i.e., Total-body PET [3]) or, by boosting the signal-to-noise ratio (SNR) of the reconstructed PET image [4,5]. The first approach constitutes a major technological challenge and requires high volumes of materials (elevated production and manufacturing costs), handling massive amounts of data and big hospital facilities thus, extending this line is not the preferred option. As an alternative, the second approach aims to effectively increase the SNR by including precise time-of-flight (TOF) information of the annihilation photons during the image reconstruction process [6]. The main parameter determining the achievable SNR is the coincidence time resolution (CTR) of the PET detectors as described by equation. 1 [7].

$$SNR_{gain} = \frac{SNR_{TOF}}{SNR_{Non-TOF}} = \sqrt{\frac{2 \bullet D}{c \bullet CTR}}$$

where D diameter of the object to be imaged and c speed of light in vacuum.

Current clinical state-of-the-art TOF-PET scanners reach <200 ps (ps) FWHM thus enable SNR gains of a factor ~ **3**.7 for D = 40 cm, with respect to the same systems without TOF capabilities [8,9].

The motivation towards further increasing the effective SNR has driven current studies to focus on improving the CTR performance of PET detectors, which requires advancements not only in the electronics and data postprocessing chains, but also in the scintillator and photo-

* Corresponding author. Department of Radiology, Molecular Imaging Program at Stanford University, Stanford, CA 94305, United States.
E-mail address: cslevin@stanford.edu (C.S. Levin).

https://doi.org/10.1016/j.net.2024.11.012
Received 15 May 2024; Received in revised form 22 October 2024; Accepted 6 November 2024
Available online 14 November 2024

sensor technologies [9–13]. Regarding the scintillator material, recent investigations proposed using materials able to produce a measurable yield of promptly emitted light photons (i.e., Cherenkov photons [14, 15]), because they are generated much faster than the scintillator's main luminescence yield, hence provide a fastest response to the incident 511 keV annihilation photons [16,17]. Note however that, the final CTR spectra contains the contribution of both Cherenkov and Scintillation photons and thus, compared with fast scintillators such as the lutetium-based ones, the global CTR obtained from BGO is still worse but competitive. Among available Cherenkov emitters, Bismuth Germanate Oxide (BGO) scintillators are the preferred option for PET imaging. Indeed, the interest on BGO has increased during the last years since it was demonstrated (laboratory level) that, by properly exploiting its fast Cherenkov luminescence component reasonably good CTR values can be obtained. For example, in Ref. [18] CTR values below 200 ps were obtained using BGO crystals with a cross-section of 3 × 3 mm^2 and lengths ranging between 3 and 20 mm coupled to Digital Photon Counting (DPC) arrays; similarly, in Ref. [19], the authors reported CTR values of 167 and 235 ps for 3 × 3 × 3 and 3 × 3 × 15 mm^3 BGO pixels when coupled to SiPMs. Note however that these values have been measured with high frequency digital readout scopes and will worsen when implementing the detector in a full system with its associated acquisition and electronics systems.

Yet, extracting useable CTR information from BGO-based detectors is not easy and, in addition to the scintillator material, requires advanced and high-sensitivity photosensor technology combined with fast and noiseless front-end electronics readouts [20] and precise data post-processing methods [17,21]. Encouragingly, recent improvements of the photodetector technology such as silicon photomultipliers (SiPMs) with good photon detection efficiency ($\boldsymbol{PDE}(\lambda, \boldsymbol{V})$) in the near ultraviolet (where Cherenkov photons are emitted [21]) and low single photon time resolution (SPTR) values have been presented [22,23]. The development of these SiPMs was a key contribution to recent improvements in TOF-PET and, the most important SiPM parameters affecting the CTR performance are [24]: the $\boldsymbol{PDE}(\lambda, \boldsymbol{V})$; the quantum efficiency ($\boldsymbol{QE}(\lambda)$); the gain, which is multiplicative factor that should be high and stable, its fluctuations is given by the Excess Noise Factor (ENF) magnitude [25]; the temperature coefficient; the linearity, which measures the response of the photodetector thus should be linear to the incident radiation; the compactness; and the time jitter, which directly relates to the timing capabilities of the system [26]. Moreover, since Cherenkov photons are emitted mostly in the UV realm [21,27], the above-mentioned factors should be optimized in the UV region of the electromagnetic spectra and, for this reason, the newest developments of SiPMs present extended $\boldsymbol{PDE}(\lambda, \boldsymbol{V})$ in the Vacuum-UV (VUV) and Near-UV (NUV) regions [22, 23]. Also, this new technology presents upgraded electric field designs in the Single-Photon Avalanche Diode (SPADs) configuration to improve the SPTR in the UV region.

This is of major relevance, since current state-of-the-art SiPM technology report $\boldsymbol{PDE}(\lambda, \boldsymbol{V})$ values between 40 and 55 % at 420 nm [28], but, the SPTR is still a remaining key parameter that need further optimization for developing clinical Cherenkov PET scanners [20]. It should be mentioned that improvements on SPTR will only be possible with parallel efforts on the electronic readout circuits [29–32] which has to reduce the influence of electronic noise to effectively exploit the Cherenkov component of the timing signal [31,32]. Additionally, specific data postprocessing methods accounting for the high fluctuations in the number of detected Cherenkov photons, which is produced by its natural non-isotropic emission [27] are also necessary for achieving useable CTR values [17,20].

Many groups have performed studies on BGO-based PET detectors (see Refs. [27–32], and references therein) showing promising results. In Ref. [13], the authors reported a CTR of 158 ± 3 ps FWHM using 22 × 3 mm^3 BGO crystals coupled to NUV SiPMs and a high frequency (HF) readout. Similarly, in Ref. [19], the authors reported CTR values of 158 ps and 277 ps FWHM, respectively, for 3 and 20 mm long BGO crystal coupled to the same NUV SiPMs. Other works focus on improving the electronic readout, such as in Ref. [20] where the authors implemented a circuitry based on a passive bootstrapping readout [30,31] that effectively reduces the SiPM device capacitance and, achieved CTR values in the range of 200–280 ps for BGO 3 × 3 × 3 and 3 × 3 × 15 mm^3 BGO crystals. More recent studies using the same SiPM technology, measured values in the range of 205–302 ps FWHM (depending on the Cherenkov yield) for 20 mm^3 long BGO using the HF readout and applying data corrections [17]. Comparable results were also reported in Ref. [32] but using UV-enhanced SiPMs from a different vendor and a custom designed circuitry. Following a different approach, other groups have shown promising progress towards using BGO in TOF-PET detectors that employ digital SiPMs (dSiPMs) instead of the analog ones [16,33]. As an example, in Ref. [29] the authors were able to assign an individual timestamp from the first detected light photon yielding ~400 ps FWHM CTR for 20 mm long BGO crystals (without any correction).

Since the photosensor technology is key to exploit the Cherenkov yield and to provide insights on the UV-enhanced SiPM technology available, the present manuscript evaluates and compares the capabilities of three pairs of UV-enhanced SiPMs that may be feasible for TOF-PET applications. In particular, we have selected the vacuum- and near-ultra-violet high density (VUV- and NUV-HD) SiPM from FBK (Trento, Italy) [34] and the NUV ones from Broadcom® [36] (details on the SiPMs are provided in the next section), since these three are the most commonly SiPMs used for BGO TOF-PET studies. Moreover, these three SiPM models have similar dimensions (matching our detector designs that uses 3 × 3 mm^2 scintillators). For the study, we have combined the SiPMs with 3 × 3 mm^2 BGO pixels (with lengths ranging from 3 to 15 mm) and two different readout circuits, namely: (i) the prototype FBK readout board [37] and, (ii) a custom designed board optimized for timing measurements [32]. Additionally, a study on the influence of the crystal surface finish (chemically etched and polished) was performed to determine the best achievable CTR with current technology. After applying state-of-the-art post-processing correction methods, best CTR performance (<300 ps CTR for 15 mm BGO scintillators) was achieved for the Broadcom® AFBR-S4N33C013 SiPMs combined with our custom readout board. Similar values were reported with the FBK NUV-HD SiPMs when combined with our custom readout board.

2. Materials and methods

Key elements to effectively exploit the Cherenkov contribution on CTR measurements are the photosensor technology, the scintillation material, the electronics readout circuit and data post-processing methods.

2.1. Photosensor: UV enhanced SiPMs

SiPMs are the most commonly used photodetectors in PET developments. SiPMs are semiconductor (solid-state) based detectors with single photon counting capabilities [25] and, to be suitable for PET systems, should present high gain with low fluctuations, high $\boldsymbol{PDE}(\lambda, \boldsymbol{V})$, high $\boldsymbol{QE}(\lambda)$, short response time (time jitter), should be compact and, as insensitive as possible to temperature fluctuations [24].

The recent developments of SiPMs with very low temperature drift, high granularity, low operating voltage and enhanced $\boldsymbol{PDE}(\lambda, \boldsymbol{V})$ in the UV range made SiPMs the ideal candidates for the detection of Cherenkov light [33,34]. Note that, Cherenkov photons yield upon the 511 keV interaction for BGO and occurs in the UV spectra, specifically the Cerenkov emission spectrum has a $\mathbf{1}/\lambda^2$ distribution, where λ is the photon wavelength, with a maximum at the BGO optical cut-off frequency at 300 nm [38]. Indeed, it has been already demonstrated that VUV- and NUV-HD SiPM technology combined with efficient data post-processing methods, make it possible to access timing information from the relatively few Cherenkov photons emitted [32,33].

Table 1
Main specifications of the SiPMs evaluated in the experiments.

Manufacturer	Model	$PDE(\lambda, V)$ at 420 nm (%)	Device Area (mm^2)	Active Area (mm^2)	Cell Size (μ m^2)	Breakdown Voltage (V)
FBK	VUV-HD Low Field	50–55	2.625 × 3.8	~ 2.6× 3.0	35	32.4
FBK	NUV-HD Low Field	50–60	3.12 × 3.2	3.0 × 3.0	40	32.4
Broadcom®	AFBR-S4N33C013	>54	3.14 × 3.14	3.0 × 3.0	30	26.9

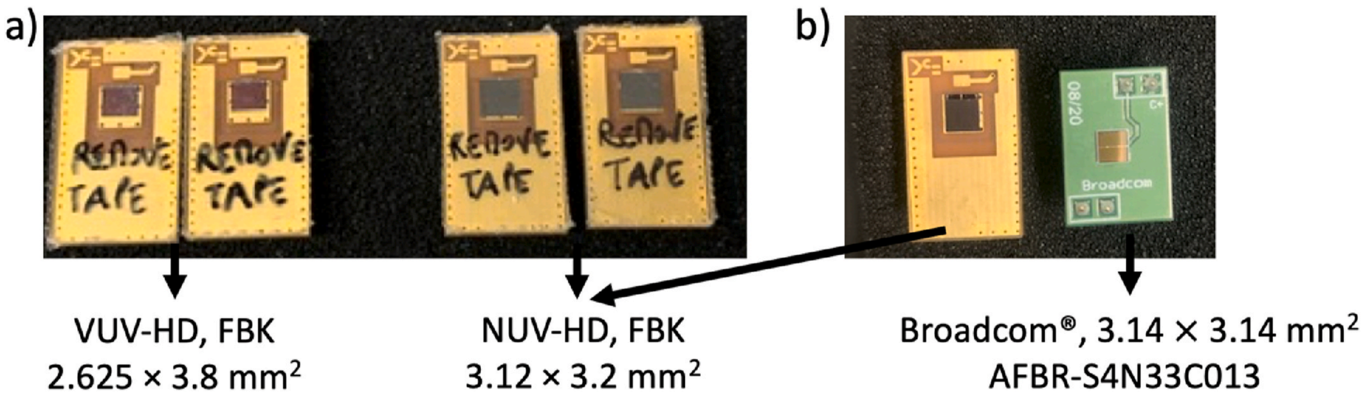

Fig. 1. (a) Photo of the two FBK models used in this work: VUV-HD and NUV-HD SiPMs. Note that, to avoid damaging the SiPMs, we didn't remove the protective layer for the photograph but, was removed for the experiments. (b) Photo comparing NUV-HD from FBK and Broadcom® AFBR-S4N33C013 devices.

In the present work we have focus on extensively evaluating three different UV enhanced SiPMs from two different providers, namely: Fondazione Bruno Kessler (FBK) and Broadcom®. The specification of each SiPM type are provided in the following and summarized in Table 1.

i. FBK, VUV-HD SiPMs, these photodetectors operate at low electric field thus, reduce the noise injected to the signals and provide precise timing measurements. These SiPMs have 35 μm^2 cell size and a device area of 2.625 × 3.8 mm^2, operate at a breakdown voltage of 32.4 V, and report a $PDE(\lambda, V)$ in the range of 50–55 % at 420 nm for bias voltages of 40–42V [34]. See Fig. 1(a) left.
ii. FBK, NUV-HD SiPMs, as the previous ones these photodetectors operate at low electric field but, have device and active areas of 3.12 × 3.2 mm^2 and 3.0 × 3.0 mm^2, respectively, with 40 μm^2 cell size, the breakdown voltage is 32.4 V and report $PDE(\lambda, V)$ values in the range of 50–60 % at 420 nm for bias voltages of 38–42V [22]. It should be pointed out that, NUV-HD technologies have two main limiting factors for direct detection in the VUV spectral range (which includes the far (400 nm) and extreme (200 nm) UV), namely: the presence of antireflective coating (ARC) not optimized for VUV light detection, and the low penetration depth of VUV photons in silicon. However, the NUV-HD SiPMs have lower correlated noise (25 % at a $PDE(\lambda, V)$ of 50 % at 420 nm) than the VUV-HD ones (35–40 % at a $PDE(\lambda, V)$ of 50 % at 420 nm [35]), thus providing enhanced capabilities for timing pick-off in the BGO's signal [34]. See Fig. 1 (a) center.
iii. Broadcom® AFBR-S4N33C013 SiPMs, with 30 μ m^2 cell size and, device and active areas of 3.14 × 3.14 mm^2 and 3.0 × 3.0 mm^2, respectively. These SiPMs achieved high packing density by using through-silicon-via (TSV) technology and a chip-sized package (CSP), report $PDE(\lambda, V)$ values > 54 % at 420 nm for bias voltages of 34–37V, excellent SPTR, and breakdown voltage at 26.9 V [36]. Moreover, the protective layer of these SiPMs is made by a glass highly transparent to UV wavelengths which results in a broad response in the visible light spectrum with high sensitivity towards blue- and near-UV regions. See Fig. 1 (b).

For the experiments, different BGO crystals (see section 2.2) were used to evaluate the performance of these SiPMs in terms of CTR, light output (Photopeak relative gain) and feasibility for detecting Cherenkov photons. In all experiments the scintillators were coupled following the end-readout configuration, to the SiPMs by means of optical grease (BC-630, Saint Gobain [39]).

2.2. Scintillator material: BGO

As a result of the primary (photoelectric or Compton) interaction of the 511 keV photons with the scintillator material, secondary electrons are emitted. These secondary electrons are able of generating Cherenkov photons along their path, with directions determined by the kinetic energy and momentum of the electron [14,15]. Most of the recoil electrons have an energy in the range of [400−500] keV and produce on average 17 Cerenkov photons [40]. The produced Cherenkov light is therefore emitted non-isotropically and, over a period of time of ~ 10 ps following the 511 keV interaction [27]. Nevertheless, the total Cerenkov emission is almost isotropic due to the multiple scattering processes that may occur and changes of direction of the recoil electrons at each scatter. Also note that, the number of Cherenkov photons that are produced depend on the scintillator properties, and in particular on its index of refraction [41].

Among available Cherenkov emitters, BGO scintillators are the preferred option for building PET detectors that employ a mixture of Cherenkov and scintillation photons. This is because BGO presents short attenuation length (1.1 cm for 511 keV photons), high effective atomic number ($\boldsymbol{Z_{eff}} = \mathbf{74}$), high density ($\boldsymbol{\rho} = \mathbf{7.13\ g/cm^3}$), and lower production cost than other scintillators [42]. Moreover, due to its high index of refraction ($\boldsymbol{n} = \mathbf{2.15}$), the 511 keV photoelectrons produce more Cherenkov photons than, for instance, the commonly used lutetium-based scintillators (~17 and ~9 above BGO's and LSO's absorption bands, respectively [5]). However, BGO-based detectors reported limited CTR performance due to their slow decay time (~45.8 ns (8 %) – 365 ns (92 %)) and low light luminescence yield (10.7–11 photons/keV) [20]. BGO's temporal signals present therefore, a fast and a slow decay component that corresponds to the emitted Cherenkov and scintillation photons [43]. Luckily, as it has been already demonstrated, by exploiting the BGO fast Cherenkov luminescence component, good CTR values can be obtained [44,45].

For the evaluation of the SiPMs described in section 2.1, we have used five different pairs of BGO crystals. In a first batch of experiments we aimed to investigate the best crystal surface finish for extracting Cherenkov information. In particular, we tested two pairs of BGO scintillators with sizes of 3 × 3 × 3 mm^2. One pair was composed of crystals with all faces chemically etched (referred as rough in this manuscript), while the other pair of BGO crystals had the six faces polished. Note that the main difference between rough and polished surfaces is the way light is reflected, in the rough surfaces the impinging rays are reflected in different directions (diffuse distribution) while in the polished surfaces the rays are reflected at the same angle as they hit the surface (specular reflections) [46]. Fig. 2 (a) and (b), provides a photograph of the different BGO crystals used in these work and explanatory sketches of the different types of light reflection (diffuse and specular), respectively.

Once determined the best surface finish, we carried out a second set of experiments to evaluate and compare the performance for each SiPM model. In particular four pair of chemically etched BGO scintillators (since this surface finish provided the best CTR results with the 3 mm^3 crystals, see Section 3.1) were used with dimensions of 3 × 3 mm^2, × 3, × 5, × 10, and × 15 mm^3, see Fig. 2 (a). In all experiments the crystals were wrapped using Teflon tape to help the reflection of the generated photons and, the face in contact with the SiPMs (3 × 3 mm^2 area) was coupled by means of optical grease. The crystals pairs used in this work and their surface finish are shown in Table 2.

Table 2
BGO scintillators used in this work, size and surface finish specifications are provided.

BGO pixel area (mm^2)	BGO pixel length (mm)	Surface finish
3 × 3	3	Polished
3 × 3	3	Chemically etched
3 × 3	5	Chemically etched
3 × 3	10	Chemically etched
3 × 3	15	Chemically etched

2.3. Electronics readout circuit

In addition to the selection of the scintillator and SiPM, exploiting the Cherenkov yield to precisely estimate the photon time of interaction, requires using low-noise and high-speed readout circuits. For the experiments reported in this work, we used two different readout boards.

i. FBK's evaluation board (Fig. 3 (a)) which includes high speed operational amplifiers (op-amp, Analog Devices, AD8000 [47]) and two output signals, namely Out_1 (with a gain of 83 V/A) and Out_2 (Pole-Zero Compensation circuit) [37]. In our experiments Out_1 was used as both energy and timing signal while Out_2 was not used. For the amplifiers, we used power supply values as for the typical configuration V_A = +5V, V_B = -5V (recommended configuration V_A -V_B = 10V).
ii. Custom readout board (Fig. 3 (b)) which is based on a passive capacitance compensation circuit as described in Ref. [32]. For the timing signal, a balun transformer (Macom MABA-007159, 50 Ω impedance [48]) was connected between the cathode and anode of the SiPM in a balanced-to-unbalanced configuration providing a 2-fold increasing pulse amplitude, to two RF amplifiers (Minicircuits MAR-6 RF Amplifier [49]) in cascade [50]. For the energy signal the SiPM anode was connected to two operational amplifiers (Analog Devices, AD8000 [47]) that were also fed with V_A = +5V, V_B = -5V. The bias voltage was carefully studied until reaching optimum performance at 5.5 V [32].

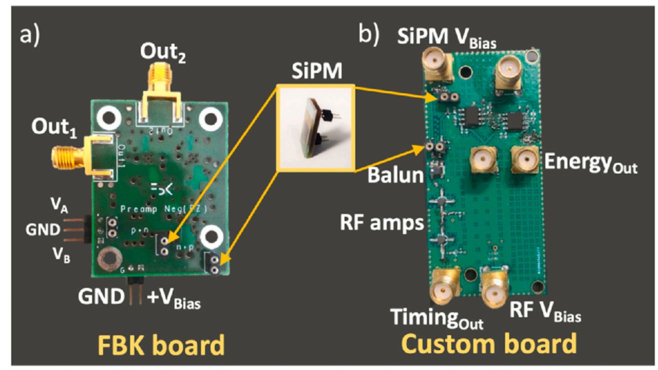

Fig. 3. (a) Photograph of the FBK's evaluation board. (b) Photograph of our custom design board which was specifically designed for timing measurements with BGO scintillators.

For coincidence data acquisition, raw waveforms from two identical detectors were acquired using a digital oscilloscope (Agilent DSO90254A 2 GHz 20 GSa/sec).

2.4. Data acquisition and analysis: postprocessing methods

During data acquisition two identical detector elements consisting on one SiPM plugged to the PCBs were used. A total of 5 SiPM-PCB configurations were tested as described in Table 3. We tested each different BGO crystal pairs (listed in Table 2) with the five SiPM-PCB configurations thus, 22 different coincidence set-ups were evaluated. In all cases, coincidence data was experimentally acquired by placing a ^{22}Na source (6 mm PMMA encapsulation, 1 mm radioactive encapsulation; 11.8 μCi activity at the time of the experiments) between two identical detectors. Three different SiPM bias voltages were tested to find the optimal acquisition condition. Note that, the mechanical considerations of the experimental set-ups (i.e., mechanics, digitizer, cables …) were identical in all cases, the distance between boards and radioactive source was maintained as well as the SiPMs connection to each of the boards. The differences between experiments are related to the voltage inputs required for each board.

Regarding the energy spectra, it was estimated as the histogram of the maximum amplitude of the collected energy waveforms, and were fitted using a Gaussian function to calculate the photopeak gain as a function of the SiPM Bias Voltage. For CTR evaluation, only events that

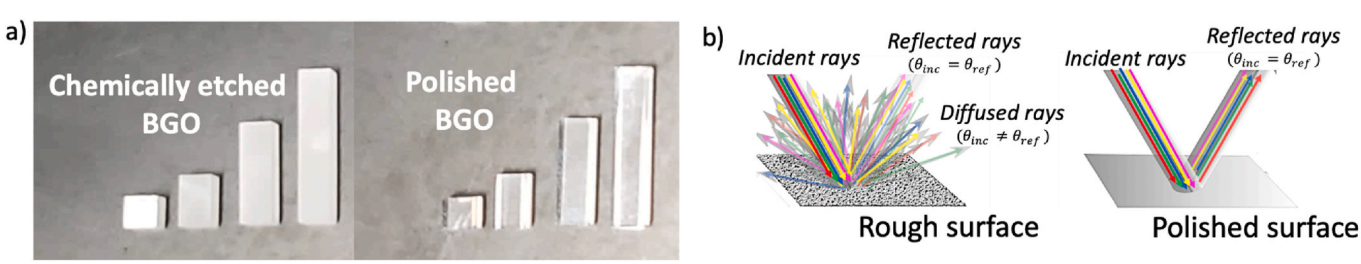

Fig. 2. (a) Photo of the different BGO pixels used in this work, element sizes are 3 × 3 × 3, 3 × 3 × 5, 3 × 3 × 10, and 3 × 3 × 15 mm^3 (from left to right). The left ones have all faces rough, and the right ones polished (only the 3 mm^3 pixel was tested for this case). (b) Sketch showing diffuse and specular reflections.

Table 3
Set-up configurations evaluated in this work.

SiPM model	PCB board	Bias Voltage, V_{Bias} (V)	Scintillator length (mm^3)
FBK VUV-HD	FBK board	37.0–38.0 – 39.0	3 × 3 × 3 Polished 3 × 3 × 3 Rough 3 × 3 × 5 Rough 3 × 3 × 10 Rough 3 × 3 × 15 Rough
	Custom board	37.0–38.0 – 39.0	3 × 3 × 3 Rough 3 × 3 × 5 Rough 3 × 3 × 10 Rough 3 × 3 × 15 Rough
FBK NUV-HD	FBK board	37.0–38.0 – 39.0	3 × 3 × 3 Polished 3 × 3 × 3 Rough 3 × 3 × 5 Rough 3 × 3 × 10 Rough 3 × 3 × 15 Rough
	Custom board	37.0–38.0 – 39.0	3 × 3 × 3 Rough 3 × 3 × 5 Rough 3 × 3 × 10 Rough 3 × 3 × 15 Rough
Broadcom® AFBR-S4N33C013 SiPMs	Custom Board	36.5–37.0 – 37.5	3 × 3 × 3 Rough 3 × 3 × 5 Rough 3 × 3 × 10 Rough 3 × 3 × 15 Rough

fell within the full-width-tenth-maximum (FWTM) of the 511 keV energy peak were considered and, both leading-edge discrimination and baseline offset correction were used to estimate the time stamp in the digitized waveforms as explained in Refs. [51,52].

Finally, since BGO's coincidence time spectrum doesn't follow a Gaussian-like distribution due the contribution of both scintillation (slow) and Cherenkov (fast) temporal components, to properly exploit the Cherenkov yield, the most relevant methods as described in the literature were included during data analysis [17], namely: (i) Rise time calculation by setting the lower threshold below one light photon equivalent level [20]; (ii) Time delay correction based on the different rise times [17,20]; and (iii) Classification correction by splitting the events into 5 × 5 regions based on their rise time. Then, each one of the 25 event categories were fitted using a double Gaussian function, and the time bias for each one was corrected using the centroid of the fast component of the distribution [32]. The corrected coincidence time spectrum was then fitted again using the same double gaussian function which provides the CTR based on only Cherenkov or only Scintillation events, as well as the convolution of both (total CTR value). Error bars were estimated as the fitting error. Finally, the Cherenkov to overall ratio was also estimated with the double gaussian fit applied to the corrected CTR spectra. As shown in equation (2) of reference [32] the implemented double gaussian function includes the term r_{Fast} which represents the abundance of Cherenkov photons.

3. Results

3.1. Rough vs polished BGO: NUV-HD and VUV-HD FBK SiPMs

This section presents the results obtained for all different crystals, when combining VUV-HD and NUV-HD SiPMs with both readout boards.

a) **3 × 3 × 3 mm^3 rough and polished BGO + VUV-HD/NUV-HD + FBK board**

Fig. 4, reports the CTR values achieved for the rough and polished 3 × 3 × 3 mm^3 BGO crystals pairs coupled to (a) the VUV-HD and (b) NUV-HD FBK SiPMs (plugged to FBK's evaluation board), as a function of the SiPM bias voltage. In the plots, the solid lines represent the raw measured CTR -without applying the corrections mentioned in Section 2.4-, while the dashed lines represent the CTR values achieved after correction. It is worth highlighting that the corrected values include both the Scintillation and Cherenkov contributions thus, no data was discarded.

Corrected CTR values of 466.9 ± 9.4 ps and 355.7 ± 8.2 ps FWHM were achieved for the polished and rough 3 × 3 × 3 mm^3 BGO crystals when coupled to the VUV-HD SiPMs, respectively. When using the NUV-

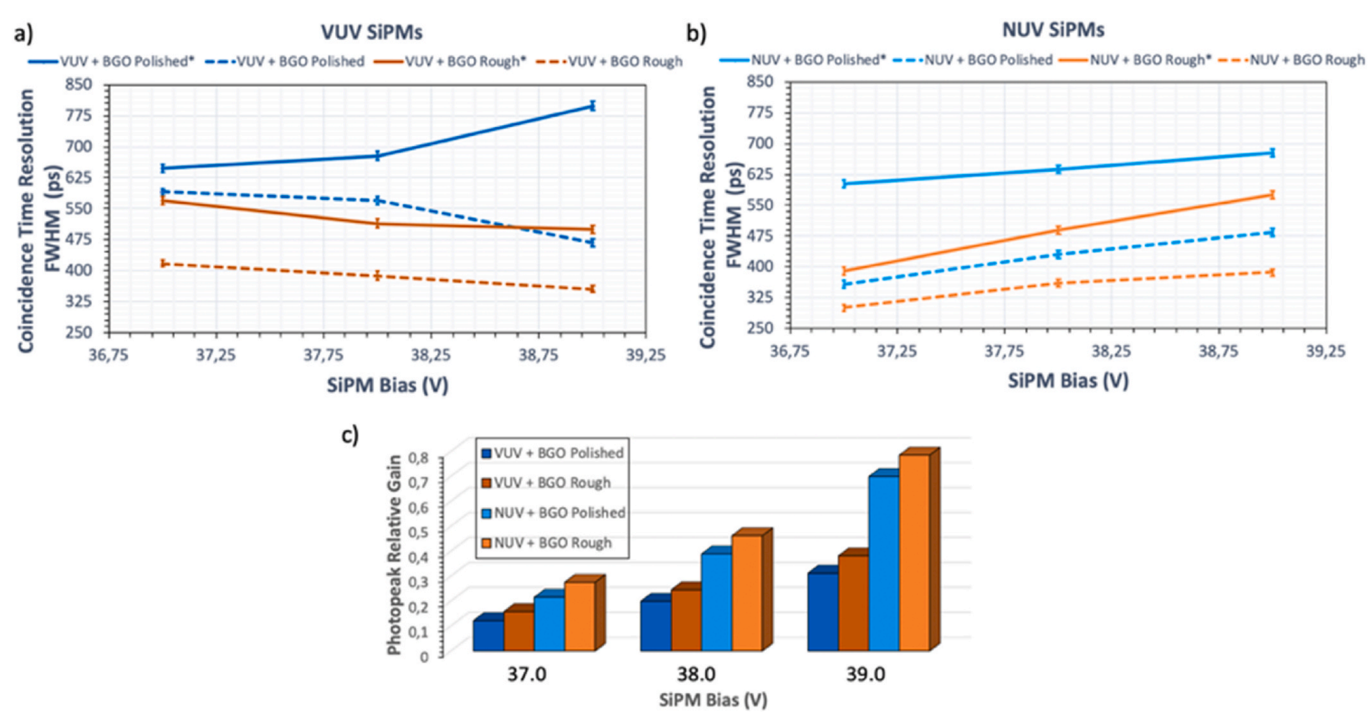

Fig. 4. CTR value measured for the 3 × 3 × 3 mm^3 rough and polished BGO crystals coupled to (a) the VUV-HD SiPMs and (b) the NUV-HD SiPMs. (c) Photopeak relative gain measured for the 3 × 3 × 3 mm^3 rough and polished BGO crystals. In the plots the solid lines represent the CTR values when no data postprocessing (corrections) were applied while the dashed ones show the CTR values after applying corrections.

HD SiPMs, these values improved to 355.7 ± 2.0 ps and 300.9 ± 1.2 ps FWHM, respectively. Thus, best corrected CTR values were achieved for the rough BGO combined with the NUV-HD technology. Regarding the Cherenkov to overall luminescence ratio in the rough BGO crystals, it was estimated to be 29.3 % and 38.2 % for the VUV-HD and NUV-HD combinations, respectively.

Fig. 4(c) shows the photopeak relative gain for each biasing voltage and SiPM-scintillator configuration. As expected, the gain increased as a function of the SiPM Bias Voltage, and the NUV-HD SIPMs reported slightly higher gains. On average, the rough BGO crystals showed an increased in the relative photopeak gain of 38 % and 67 % with respect to the polished ones for the VUV-HD and NUV-HD SiPMs, respectively. Based on these results, rough BGO scintillators were selected for the next experiments.

b) **3 × 3 ×3, 5, 10 and 15 mm^3 Rough BGO + VUV-HD/NUV-HD + FBK board**

The left and right plots in Fig. 5 depict the CTR values before (solid lines) and after (dashed lines) applying the corrections outlined in Section 2.4, for the VUV-HD and NUV-HD SiPMs (both plugged to FBK's evaluation board) data, respectively. From to bottom, the CTR values achieved for the different BGO crystal lengths of 3, 5, 10 and 15 mm are shown.

Best corrected CTR values of 309.1 ± 9.1, 474.2 ± 10.1, 523.0 ± 9.1, and 697.8 ± 10.3 ps FWHM were achieved for the VUV-HD SiPMs and of 302.7 ± 9.3, 435.2 ± 11.4, 444.3 ± 8.9 and 542.8 ± 10.4 ps FWHM for the NUV-HD SiPMs for the 3 × 3, × 3, × 5, × 10, and × 15 mm^3 rough BGO crystals, respectively. Hence, using the NUV-HD devices instead of the VUV-HD ones provides CTR improvements of 2 %, 8 %, 15 % and 22 % for the 3, 5, 10, and 15 mm long rough BGO crystal pixels, respectively. Regarding the Cherenkov to overall luminescence ratio values of 29.3 %, 21.6 %, 20.4 % and 18.4 % were estimated for the 3, 5, 10 and 15 mm long crystals when coupled to the NUV-HD SiPMs.

Fig. 6 (a) and (b) report for each rough BGO crystal length, the photopeak relative gain as a function of the SiPMs Bias Voltage, measured for the VUV-HD and NUV-HD SiPMs plugged to the FBK board, respectively. On average, an increased relative photopeak gain of

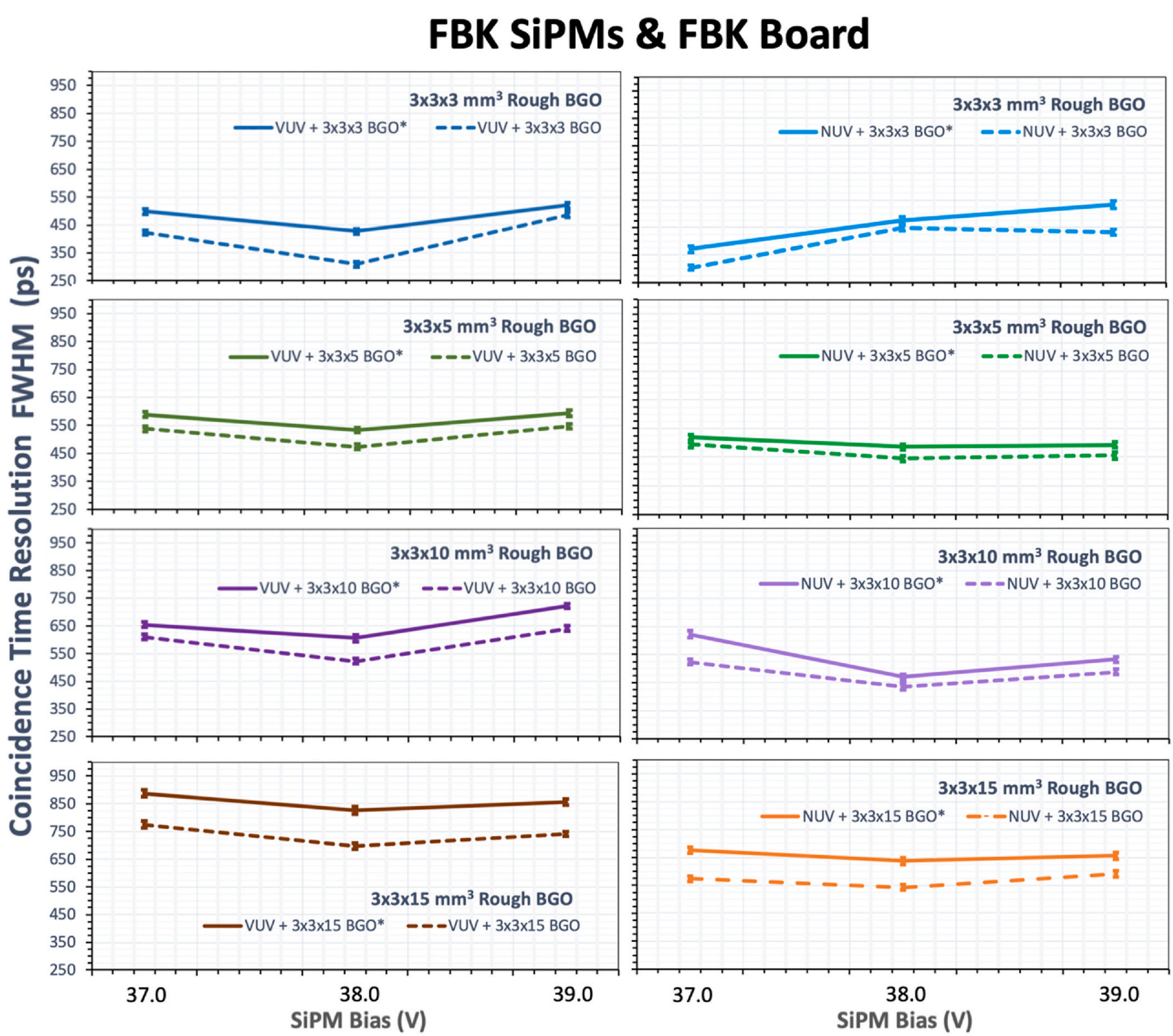

Fig. 5. CTR values before (solid lines) and after (dashed lines) applying corrections for the VUV-HD (left) and NUV-HD (right) SiPMs data, when using FBK's readout board. The CTR values achieved for the different BGO lengths of 3, 5, 10 and 15 mm are shown from top to bottom.

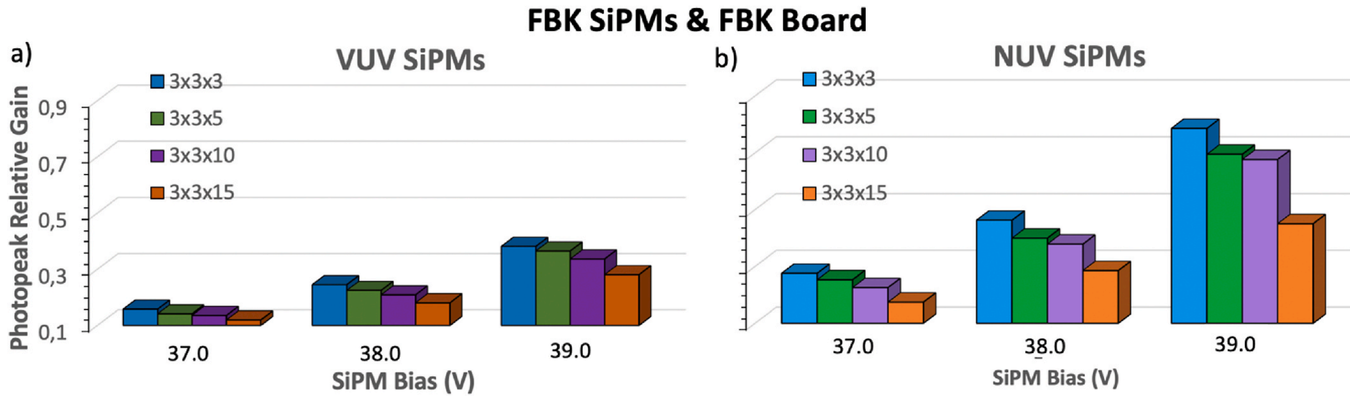

Fig. 6. Photopeak relative gain measured for the (a) VUV-HD and (b) NUV-HD SiPMs plugged to the FBK evaluation board, as a function of the SiPMs Bias Voltage for each rough BGO crystal length.

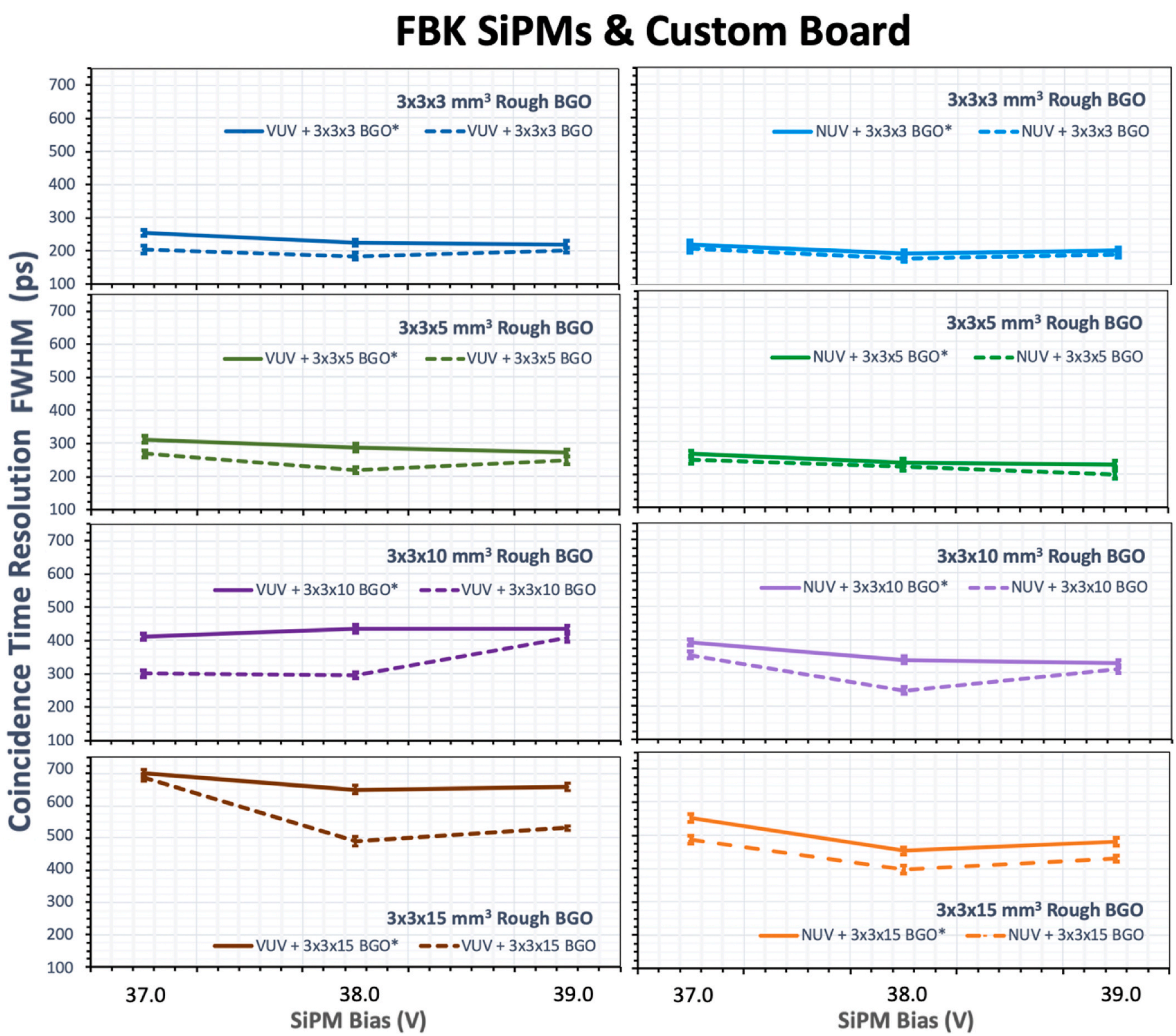

Fig. 7. CTR values before (solid lines) and after (dashed lines) applying the corrections for the VUV-HD (left) and NUV-HD (right) SiPMs data, respectively, when using our custom readout board. The CTR values achieved for the different BGO lengths of 3, 5, 10 and 15 mm are shown from top to bottom.

approximately 42 % was achieved when using the NUV-HD SiPMs instead of the VUV-HD ones. As expected, the gain increases as a function of the SiPM bias voltage, and, the smaller the scintillator cross section, the higher gains. Also, the photopeak relative gain decreases as a function of the crystal length due to a worse light collection efficiency and losses due to the reflections of the light inside the crystal [46].

c) **$3 \times 3 \times 3$, 5, 10 and 15 mm^3 Rough BGO + VUV-HD/NUV-HD + Custom board**

Fig. 7 provides the CTR results measured when plugging the FBK SiPMs to our custom readout board which was specifically designed for exploiting the Cherenkov contribution to the CTR histogram [32]. As a function of the SiPM Bias Voltage, the left and right panels in Fig. 7 report the raw non-corrected (solid lines) and corrected (dashed lines) CTR values for the VUV-HD and NUV-HD SiPMs data, respectively. From top to bottom, the CTR values achieved for the different BGO lengths of 3, 5, 10 and 15 mm are shown.

Best corrected CTR values of 183.9 ± 10.3, 219.4 ± 10.8, 294.9 ± 8.6, and 490.2 ± 14.1 ps FWHM and of 182.5 ± 10.0, 198.4 ± 11.2, 247.2 ± 10.4 and 397.1 ± 12.4 ps FWHM were reported for the $3 \times 3 \times 3$, 5, 10, and 15 mm^3 rough BGO when coupled to the VUV-HD and the NUV-HD SiPMs, respectively. The NUV-HD devices provide CTR improvements of 1 %, 9 %, 16 % and 19 % over the VUV-HD ones, for the 3, 5, 10, and 15 mm long rough BGO pixels, respectively. Regarding the Cherenkov to overall luminescence ratio values of 38.2 %, 35.4 %, 34.4 % and 25.1 % were estimated for the 3, 5, 10 and 15 mm long crystals coupled to the NUV-HD SiPMs.

The measured photopeak relative gain for the VUV-HD and NUV-HD SiPMs plugged to our custom board are shown as a function of the SiPMs Bias Voltage in Fig. 8 (a) and (b) respectively, for each rough BGO crystal length. On average an increased relative photopeak gain of approximately 51 % was achieved with the NUV-HD SiPMs.

d) **VUV-HD/NUV-HD SiPMs, summary**

Table 4 summarizes the best achieved corrected CTR values for both the VUV-HD and NUV-HD SiPMs and for each rough BGO crystal length. The reported results include the values measured using the FBK board and our custom board. Best CTR performance was achieved for the configuration using rough BGO + NUV-HD SiPMs + Custom readout board.

Similarly, Table 5 reports the photopeak relative gain measured at 38V for the configurations described in Table 4. As expected, the NUV-HD SiPMs combined with the custom readout board yields the highest gains.

Table 4
Best corrected CTR values for the VUV-HD and NUV-HD SiPMs and for each rough BGO crystal length. Results are reported for both the FBK and custom boards.

SiPM	Board	Rough BGO dimension			
		$3 \times 3 \times 3$ mm^3	$3 \times 3 \times 5$ mm^3	$3 \times 3 \times 10$ mm^3	$3 \times 3 \times 15$ mm^3
VUV-HD	**FBK**	309.1 ± 9.1 ps	474.2 ± 10.1 ps	523.0 ± 9.1 ps	697.8 ± 10.3 ps
NUV-HD	**FBK**	302.7 ± 9.3 ps	435.2 ± 11.4 ps	444.3 ± 8.9 ps	542.8 ± 10.4 ps
VUV-HD	**Custom**	183.9 ± 10.3 ps	219.4 ± 10.8 ps	294.9 ± 8.6 ps	490.2 ± 14.1 ps
NUV-HD	**Custom**	182.5 ± 10.0 ps	198.4 ± 11.2 ps	247.2 ± 10.4 ps	397.1 ± 12.4 ps

Table 5
Photopeak relative gain measured for the configurations reporting the best CRT values.

SiPM	Board	Rough BGO dimension			
		$3 \times 3 \times 3$ mm^3	$3 \times 3 \times 5$ mm^3	$3 \times 3 \times 10$ mm^3	$3 \times 3 \times 15$ mm^3
VUV-HD	**FBK**	0.25	0.22	0.20	0.18
NUV-HD	**FBK**	0.46	0.40	0.38	0.29
VUV-HD	**Custom**	0.30	0.26	0.24	0.18
NUV-HD	**Custom**	0.70	0.61	0.50	0.40

3.2. Rough BGO + Broadcom® AFBR-S4N33C013 SiPMs + custom readout

In the following, only the custom readout board was used (with the Broadcom® SiPMs) since it reported better CTR performance than the FBK.

a) $3 \times 3 \times 3$, 5, 10 and 15 mm^3 Rough BGO + Broadcom® SiPMs + Custom board

Fig. 9 (a) depicts the average CTR values achieved, as a function of the SiPM Bias voltage, for each one of the different BGO pairs when coupled to Broadcom® AFBR-S4N33C013 SiPMs. Results are provided before (solid lines) and after (dashed lines) applying the corrections outlined in Section 2.4. After correction, best CTR values of 155.7 ± 7.1, 187.9 ± 9.0, 229.7 ± 9.0 and 297.9 ± 9.1 for the 3, 5, 10, and 15 mm

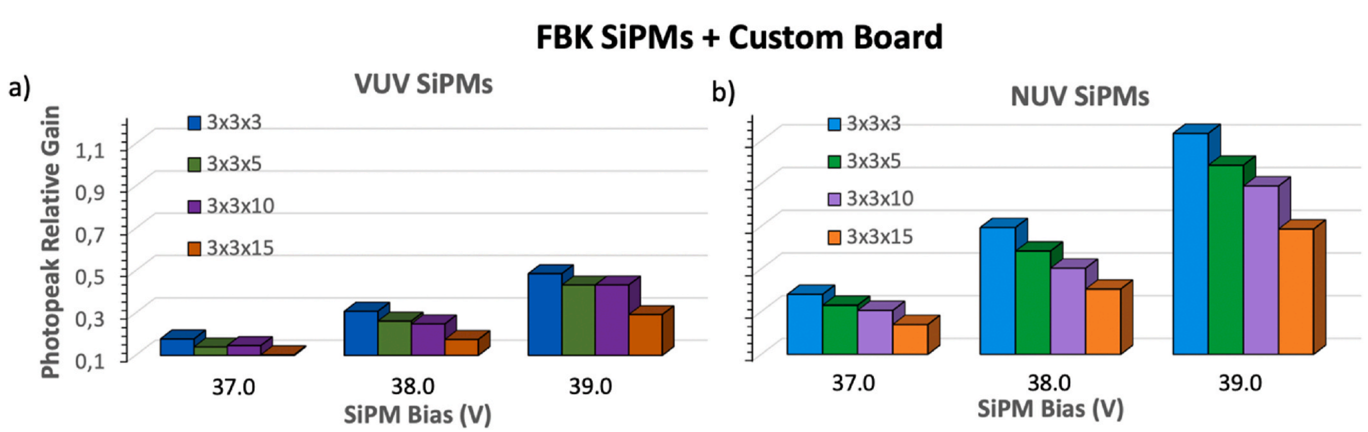

Fig. 8. (a) Photopeak relative gain measured as a function of the SiPMs Bias Voltage for the VUV-HD and (b) NUV-HD SiPMs plugged to the custom board, for each rough BGO crystal length.

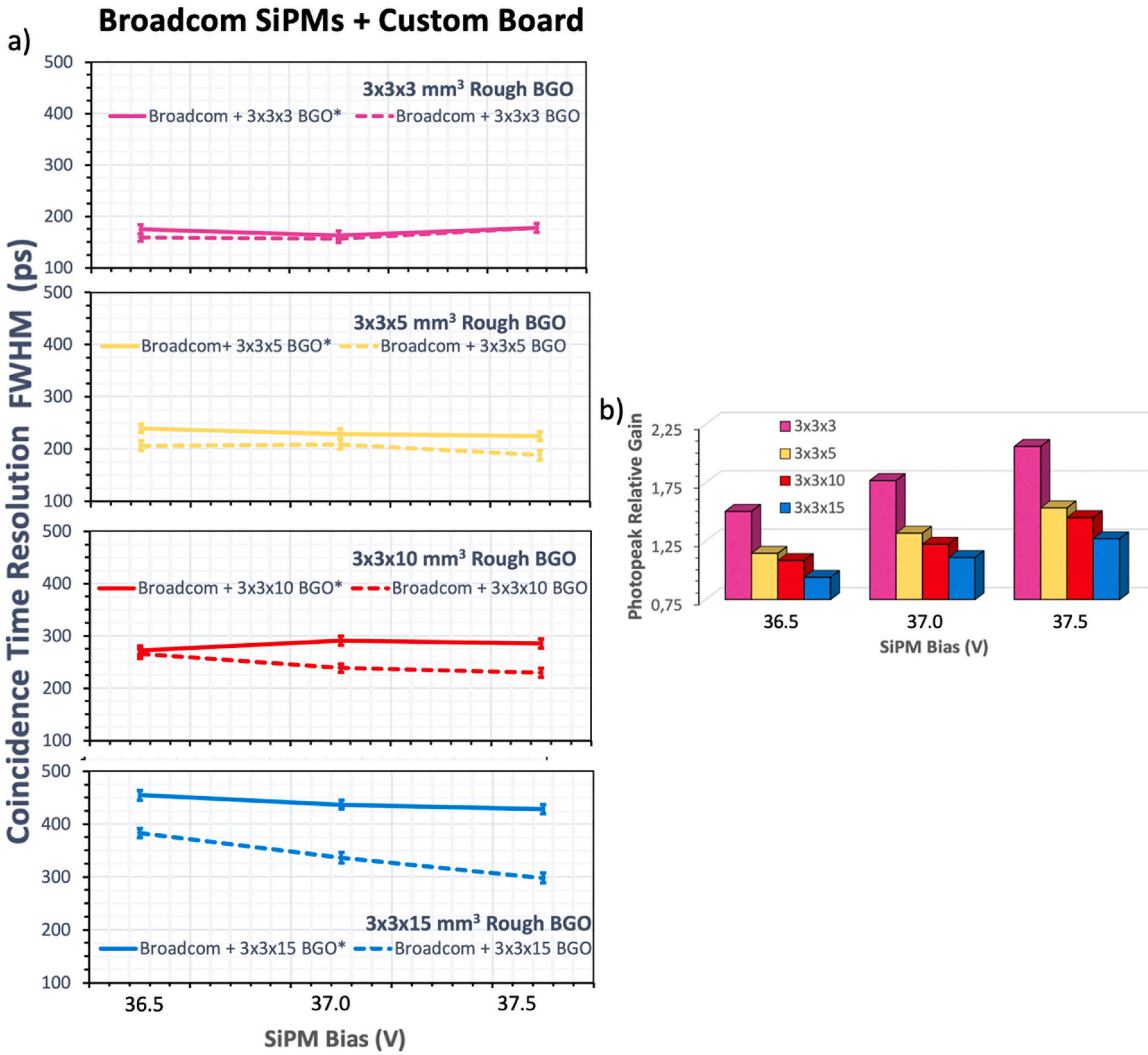

Fig. 9. (a) From top to bottom, CTR values before (solid lines) and after (dashed lines) applying the corrections for the different BGO lengths of 3, 5, 10 and 15 mm coupled to the Broadcom® AFBR-S4N33C013 SiPMs and plugged to our custom readout board. (b) Photopeak relative gain measured for the Broadcom® AFBR-S4N33C013 SiPMs for each different BGO length.

length BGO crystals respectively. In this case, the Cherenkov to overall luminescence ratio (after applying the mentioned energy filter thus only events that fell within the FWTM of the 511 keV energy peak were considered) was estimated to be of 36.4 %, 33.3 %, 31.4 % and 27.5 % for the 3, 5, 10 and 15 mm long crystals.

Fig. 9 (b), right shows the photopeak relative position at each biasing voltage and for each scintillator length. Highest gains were reported for the smallest ($3 \times 3 \times 3$ mm^3) BGO crystals at 37.5 V.

3.3. *Performance comparison: FBK/Broadcom® SiPMs*

To provide at a "one glance" comparison of the CTR performance achieved by each SiPM model, Fig. 10 summarizes the best CTR FWHM values (corrected) measured for each one of the described configurations, namely: VUV-HD + FBK board, NUV-HD + FBK board, VUV-HD + Custom board, NUV-HD + Custom board and, Broadcom® AFBR-S4N33C013 + Custom Board, and for each $3 \times 3 \times$ (a) 3, (b) 5, (c) 10 and (d) 15 mm^3 rough BGO pairs length.

Table 6 summarizes the best corrected CTR values reported for the VUV-HD, NUV-HD and Broadcom® SiPMs when coupled to the custom readout board. Best values are obtained for the configuration using rough BGO + Broadcom® AFBR-S4N33C013 SiPMs + Custom readout board. Considering only the best two cases, the NUV-HD and Broadcom® AFBR-S4N33C013 SiPMs, an improvement of ~ 11 % is obtained on average when using the Broadcom® SiPMs while the measured Cherenkov ratios reported deviations <5 %.

4. Discussion

In this work, we have investigated and compared the CTR performance of three different SiPM models with enhanced properties in the UV regions where Cherenkov photons are mostly emitted. In particular,

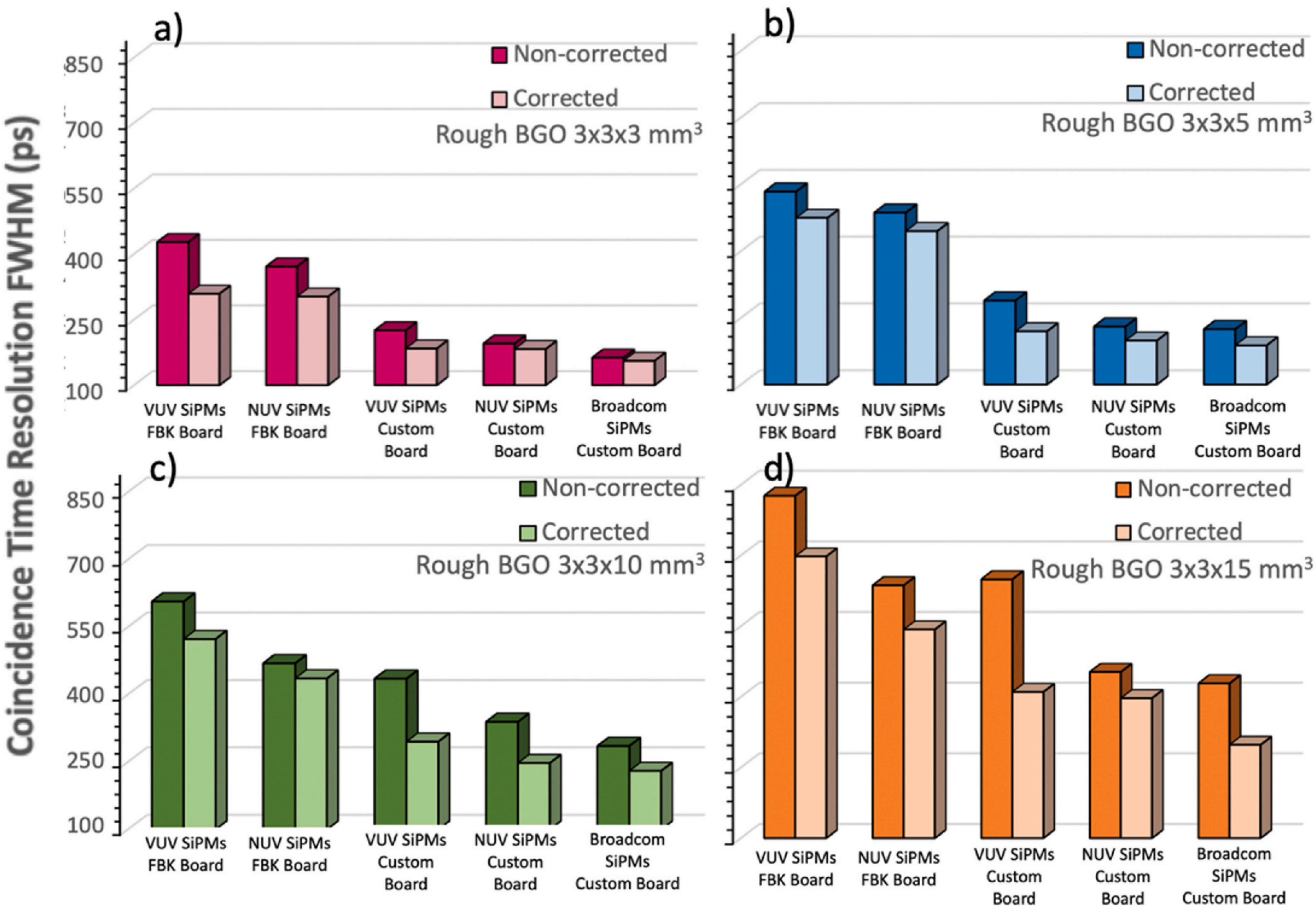

Fig. 10. (a) Best CTR values for the 3 × 3 × (a) 3, (b) 5, (c) 10 and (d) 15 mm^3 rough BGO pairs. Results are provided for each SiPM + Board configuration. The dark bars represent the non-corrected data while the lighter ones depict the corrected CTR values.

Table 6
Best FWHM CTR values obtained for each different crystal after correcting the data for each described configuration.

SiPM	Board	Rough BGO dimension			
		3 × 3× 3 mm^3	3 × 3× 5 mm^3	3 × 3 × 10 mm^3	3 × 3 × 15 mm^3
		CTR (ps)			
VUV-HD	**Custom**	183.9 ± 10.3 ps	219.4 ± 10.8 ps	294.9 ± 8.6 ps	490.2 ± 14.1 ps
NUV-HD	**Custom**	182.5 ± 10.0 ps	198.4 ± 11.2 ps	247.2 ± 10.4 ps	397.1 ± 12.4 ps
AFBR-S4N33C013	**Custom**	155.7 ± 7.1 ps	187.9 ± 9.0 ps	229.7 ± 9.0 ps	297.9 ± 9.1 ps

we have tested the VUV-HD and NUV-HD SiPMs from FBK, and the AFBR-S4N33C013 SiPMs from Broadcom®. These three models have similar active areas of ~ 3× 3 mm^2 and $\boldsymbol{PDE}(\lambda, \boldsymbol{V})$ values in the range of 50–55 % at 420 nm. However, the microcell (SPADs) size and configuration, breakdown voltage and hardware components are different.

In particular, our study focused on evaluating the CTR that can be achieved by properly exploiting the low Cherenkov yield present in BGO scintillators and thus, design a TOFPET detector able to provide an increased SNR. With this goal, a total of 22 data-sets were acquired by combining the three mentioned SiPMs models with two different readout boards, and BGO crystals of 3 × 3 mm^2 with lengths of 3, 5, 10 and 15 mm. Additionally, we have studied the influence of the crystal surface finish on the Cherenkov light extraction by testing 3 × 3 × 3 mm^3 BGO crystals, first with all faces polished and then, with all faces rough.

The 22 data sets were postprocessed using the methods mentioned in Section 2.4. These corrections are mandatory to account for the non-gaussian shape of BGO's coincidence time spectrum, since the CTR histogram doesn't follow a Gaussian-like distribution, indeed, it presents tails that arise from events where one or both detectors do not detect any Cherenkov photons. It has been estimated that, depending on the SiPM properties and crystal surface finish, for short scintillators the percentage of coincidence events where both detectors (in the following referred as Det_1 and Det_2) collect one Cherenkov photon is ~60 % while for crystal lengths >15 mm this value reduces to 30–40 % [26]. As a result, the CTR distribution has four components: (i) Cherenkov photon in both detectors (Cherenkov in Det_1 and Det_2), (ii) at least one Cherenkov photon in one detector (Det_1) and a scintillation photon in its coincidence detector (Det_2), (iii) at least one Cherenkov photon in the other detector (Det_2) and a scintillation photon in its coincidence detector (Det_1), and (iv) no Cherenkov photons in either detector. Thus, to exploit the Cherenkov contribution and achieve good CTR using BGO scintillators, the outlined methods are mandatory.

Regarding the crystal surface finish experiments, better results were achieved for the rough BGO. Note that these tests were performed using the Out_1 of the FBK evaluation board (see Section 2.3) which is not optimized for timing purposes. However, this was the only readout available at the moment of the experiments and is still suitable for providing a fair comparison between the two BGO crystal surface finish. The better CTR achieved for the rough case compared to the polished one, is due to the fact that rough surfaces minimize the light transit time in the scintillation crystal before hitting the SiPM [53]. Also, roughened surfaces combined with Teflon-tape have demonstrated to provide a diffusive reflection of the light which implies a better light output and a reduced number of photons being trapped in the crystal as described in Refs. [53,54]. Note that these results are in good agreement with the ones previously reported in the literature, for example in Ref. [43], the authors simulated four BGO crystal thicknesses ranging from 5 to 20 mm, with three crystal cross-sections (2×2, 3×3, and 6×6 mm^2) having roughened or polished surfaces. They conclude that, when considering thinner materials and larger cross-sections, using rough surfaces produces an increase in the number of Cerenkov photons detected per gamma event which led to a slightly better detection time compared to the polished case. More recently, in Ref. [55] the authors demonstrated though an experimental study using a $50 \times 50 \times 2$ mm^3 BGO detector that substituting the polished for rough surfaces leads to an overall increase in photon collection efficiency of 34 % (including the Cherenkov photon collection efficiency) which results in a reduction of the photon detection delays of the first few optical photons and thus, a better CTR. As a consequence of our results (that match with previous works), we decided using rough BGO crystals for the comparison performance of the three SiPM models as a function of the crystal length.

For the SiPM comparison experiments, we tested BGO crystal elements of $3 \times 3 \times 3$, $3 \times 3 \times 5$, $3 \times 3 \times 10$, and $3 \times 3 \times 15$ mm^3, with rough (chemically etched) surfaces and wrapped using Teflon tape. In all these 20 set-ups, to enhance the transmission of light to the photosensor, the scintillators were coupled by one of its short sides (3×3 mm^2) to the SiPM using optical grease. For coincidence measurements, two identical detector elements were used in each case. Note that, each FBK SiPM + scintillator configuration was tested using both the FBK evaluation board and our custom designed board but, the configurations using the Broadcom® AFBR-S4N33C013 SiPMs were only tested using our board. Concerning the different response obtained with the electronics boards, it should be mentioned that in addition to the digitizer (in our case an Agilent DSO90254A 2 GHz 20 GSa/sec oscilloscope), the preamplification chain is also affecting the detector performance in terms of timing capabilities. Based on the observed performance and the fact that we are using a very low-noise (noise Fig. 2.3 dB), high-performance (gain of 1.8 dB typ. at 0.1 GHz) oscilloscope, we hypothesize that the noise induced by the digitizer is minimal in comparison to the one related to the electronic components of the PCBs (FBK's and custom readout) and their capabilities to preserver the rise time of the signals. Moreover, to prevent performance discrepancies produced by other elements of the acquisition chain during the evaluation of the FBK and custom readouts, the same oscilloscope channels, the same cables and also the same FBK SiPMs were used in the two boards thus, only the PCB and cable-connections were different. Therefore, we envisage that the reported differences in timing performance reported by the two readouts are mostly related to the electronics chain. Note that in the FBK evaluation board the same signal (sent to the preamplifier in DC mode) with the same amplification chain was used for both energy and timing measurements, this chain incorporates an AD8000 operational amplifier and includes a feedback resistance of 1 kΩ together with a 20 Ω decoupling resistance [57]. This configuration provides large signals (long-tail effect as reported in Ref. [57]) which are mostly produced by the signal recovery time due to the single cell capacitance and the quenching resistor (this effect can be mitigated using a pole-zero cancellation circuitry but in our case was not efficient for the BGO scintillators).

In the custom readout, the preamplification scheme of the FBK board was also used but only for the energy channel. The timing channel (output signal from the SiPM anode) includes an optimized amplification chain based on two Minicircuits MAR-6 RF Amplifiers in cascade. Therefore, while the energy branch is comparable to the FBK's one (but inverted), the optimized timing branch of the custom PCB allows for a better preservation of the sharp nature of the temporal signals and thus its fast response [32], which yields better timing performance.

Table 6 summarizes the best achieved CTR values (after corrections) for each crystal length and SiPM model. As can be seen better results were achieved for the configuration using rough BGO crystals + Broadcom® AFBR-S4N33C013 SiPMs + Custom readout board. On average, considering all crystal lengths, improvements of $\sim$ 11 % and $\sim$ 24 % are obtained when using the Broadcom® SiPMs instead of the NUV-HD and VUV-HD ones, respectively. The measured Cherenkov ratios reported deviations <5 %. We think that the difference in the results is due to the slightly higher $\boldsymbol{PDE}(\lambda, \boldsymbol{V})$ of the Broadcom® devices as well as the protective layer of these SiPMs which is made by a glass highly transparent to UV wavelengths. To confirm this hypothesis, our future work includes testing the recently presented high performance metal filled (MT) trench NUV-MT devices. These new SiPMs present higher sensitivity than the previous ones, which ranges from the NUV to the red wavelengths of the light spectrum and report values up to 63 % $\boldsymbol{PDE}(\lambda, \boldsymbol{V})$ at 420 nm. The MT technology may enable a reduction of correlated noise (cross-talk) and of the dark count rate by more than a half compared to NUV-HD [56]. It has to be mentioned that, the slightly worse performance reported with the VUV-HD SiPMs may be also influenced by its smaller active area of 2.6×3.0 mm^2 compared to the 3.0×3.0 mm^2 of the other two SiPMs, since the coupling surface ratio has an important impact on the amount of collected light and thus on timing performance.

It will also be of interest the investigation of Hamamatsu devices since they are one of the most widely used SiPMs and have already demonstrated good timing performance when coupled to BGO scintillators.

For example, the Hamamatsu series NUV 13360, VUV S13370 and S14160 have been already investigated for exploiting the Cherenkov contribution within TOF-PET applications.

The NUV S13360 [57,58] and VUV S13370 [59] SiPMs series with an active area of 3×3 mm^2 have reported maximum sensitivity peaks at 410 nm reaching PDE values of 62 %. Moreover, the last devices (4th generation VUV4) from the Hamamatsu VUV S13370 series include a quartz window (instead of the traditional epoxy or silicon ones) with a refractive index >1.55 which may enhance the collection of Cherenkov photons [60].

Similarly, the S14160 and S14161 series [61] with an active area of 3×3 mm^2, reported PDE values of 60 % at 410 nm [e] and good timing performance. With the S14160, CTR values of 159 and 326 ps FWHM have been already reported (exploiting the Cherenkov contribution) when coupled to $2 \times 2 \times 3$ and 3x3x20 mm^3 BGO pixels, respectively. These values are comparable with the ones reported in setups using FBK and Broadcom SiPMs as shown in Refs. [17,62]. For instance, in Ref. [17], the authors provide a comprehensive study comparing the performance of both the S13360 and S14160 SiPM series with other devices for total body PET systems. They used BGO crystals with cross sections of 1×1, 2×2 and 3×3 mm^2 and lengths ranging from 3 to 30 mm, concluding that, in general terms, SiPMs from Hamamatsu benefit from extended PDE at longer wavelengths (i.e., slightly higher PDE weighted over the Cherenkov emission) but their SPTR performance is slightly worse than the one reported from other vendors such as FBK. More recently, the S14161 SiPMs have been also studied for the implementation of dual-ended readouts for 20 mm thick BGO scintillator matrixes [63].

Based on these works and some others that can be found in the literature, the Hamamatsu devices are potential candidates for the development of PET scanners aiming to exploit the Cherenkov contribution and thus, should be considered as an alternative to the ones proposed in this work.

Focusing on our best results, the Broadcom® devices yielded to non-corrected CTR values in the range of 160–430 ps for crystals ranging from 3 to 15 mm. These values improved to the range of 155–298 after correction, thus highlining the importance of properly accounting for the different contributions in the BGO's CTR histogram. As expected the CTR performance worsen as a function of the crystal length [32], to account for this it has been already proposed coupling the scintillators by one of its long sides to an array of SiPMs [33]. This is the so-called side readout approach and, has demonstrated to reduce the transit time variance of the photons to the photosensor while enhancing the light collection efficiency. The main challenge in this configuration is how to properly combine the SiPMs signal without increasing the effective capacitance of the device and thus, the electronic noise.

Summarizing, there are promising approaches for extending the BGO-PET detector concept to a clinical TOF-PET scanner which are further encourage by our work. The presented results compare the capabilities of current SiPM technology with enhanced performance in the UV region. As shown, the SiPM models tested are promising devices in this regard since allows to efficiently exploit the low Cherenkov yield resulting in good CTR values using BGO scintillators of different lengths.

We would like to highlight that, the new advances in scintillators and detector technology have encourage the research community to investigate different solutions for BGO-TOF-PET. As an example, in Ref. [64] the authors proposed using metascintillators. This consists on composite crystal topologies comprising of multiple scintillating and light-guiding materials. In particular, they constructed a metapixel based on eight pairs of $3 \times 3 \times 0.25$ mm^3 BC-422 and $3 \times 3 \times 0.2$ mm^3 BGO pixels and prove that it is possible to detect the extent of energy sharing by comparing the pulse amplitude and achieve good CTR values [64]. Similarly, in Ref. [65] the authors constructed a BGO + BC-422 $3.8 \times 3.8 \times 3$ mm^3 pixel that yielded a CTR of 95 ps for one third of the events depositing 511 keV while the rest of the 511 keV events perform like standard BGO crystals with a CTR of 165 ps. Other approaches proposed different Cherenkov emitters than BGO such as in Ref. [66] where it is proposed using lead fluoride instead of BGO in a Cherenkov-based PET scanner. Finally, it is worth mentioning that a parameter to be studied in our research is the effect of the coupling material between the SiPMs and the crystals. It is difficult finding coupling materials with limited absorption and reflection in the UV region [45]. We would like to replace the optical greasy by glycerin or optical silicone.

5. Conclusion

The present work reports and compares the performance of three SiPM models with similar active areas and enhanced capabilities in the UV region. In particular, we have evaluated the VUV- and NUV-HD SiPMs from FBK [22,34] and the NUV AFBR-S4N33C013 from Broadcom® [36] in terms of CTR performance when using scintillator that provide a mixture of Cherenkov and scintillation photons. Also, the relative gain of the photosensors has been compared since this is related to the energy and timing resolutions.

Before focusing on the SiPMs performance, we evaluated the influence of the crystal surface finish (rough and polished sides) on CTR performance by using $3 \times 3 \times 3$ mm^3 BGO crystals combined with both the VUV- and NUV-HD FBK SiPMs coupled to the FBK evaluation PCB board (since was the only one available at that moment). Results show that rough (chemically etched) surfaces are most suitable for TOF-PET since they yielded better CTR and higher gains.

Once the BGO surface finish was settled, the three SiPM models were tested using rough BGO scintillators with different sizes of: $3 \times 3 \times 3$, $3 \times 3 \times 5$, $3 \times 3 \times 10$, and $3 \times 3 \times 15$ mm^3. The SiPMs were evaluated using our custom designed PCB board that was specifically designed for timing measurements [32]. Additionally, the FBK evaluation board was used in combination with the FBK SiPMs to ensure that no impedance mismatching was produce when using our electronics. The timing performance differences observed between the electronic boards are mostly produced by the preservation of the signal rise time, which is better in the case of the custom readout board.

Best CTR values, which already include all the state-of-the-art data postprocessing methods that are commonly used to exploit the Cherenkov contribution to the CTR, were reported for the Broadcom® AFBR-S4N33C013 + Custom Board configuration. These values are similar to those measured by the NUV-HD + Custom board configuration which shows on average a degradation of about 11 % on CTR performance.

The results presented here demonstrate that currently available SiPMs technology with enhanced performance in the UV region are a good candidate for designing BGO-based PET detectors with CTR performance equivalent to or better than current state-of-the-art in TOF-PET [8,9].

CRediT authorship contribution statement

Andrea Gonzalez-Montoro: Writing, review & editing, Software, Experiments, Methodology, Investigation, Data analysis, Data curation, Supervision. **Shirin Pourashraf:** Methodology (especially, electronics), Investigation, Experiments. **Stefano Merzi:** Methodology (especially electronics), Investigation, Interpretation of results. **Alberto Gola:** Methodology (especially electronics), Investigation, Interpretation of results. **Craig S. Levin:** Planning of experiments, Interpretation of results, Writing, reviewing & editing, Validation, Supervision, Project administration.

Funding

This work was supported by NIH grants R01CA214669 and R01EB025125. Andrea Gonzalez-Montoro was partially supported by VALi + d Program for Researchers in Postdoctoral Phase of the Ministry of Labor and Social Economy (Generalitat Valenciana) and the EU Social Fund.

Declaration of competing interest

The authors declare that they have no known competing financial interests or personal relationships that could have appeared to influence the work reported in this paper.

Acknowledgments

The authors would like to thank Stefan Brunner from Broadcom® for providing the SiPM samples used in this study.

The authors would like to thank Stefano Merzi, Alberto Gola, and Giacomo Borghi from FBK for providing the SiPM samples used in this study and for the thoughtful discussion regarding achieved performance.

The authors would also thank Dr. Shirin Pourashraf for her contribution designing the custom PCB board used in the experiments as well as her support during data collection; and to Dr. Joshua Cates for his contribution in the initial implementation of the code used for data correction and thoughtful comments.

References

[1] S. Vandenberghe, P. Moskal, J.S. Karp, State of the art in total body PET, EJNMMI Phys 7 (2020) 35.
[2] L. Huo, N. Li, H. Wu, et al., Performance evaluation of a new high-sensitivity time-of-flight clinical PET/CT system, EJNMMI Phys 5 (2019) 29.
[3] S.R. Cherry, T. Jones, J.S. Karp, et al., Total-body PET: maximizing sensitivity to create new opportunities for clinical research and patient care, J. Nucl. Med. 59 (1) (2017) 3–12.
[4] P. Lecoq, C. Morel, J.O. Prior, et al., Roadmap toward the 10 ps time-of-flight PET challenge, Phys. Med. Biol. 65 (2020) 21RM01.
[5] W.W. Moses, Recent advances and future advances in time-of-flight PET, Nucl. Instrum. Methods Phys. Res. A 580 (2007) 919–924.
[6] D.R. Schaart, G. Schramm, J. Nuyts, S. Surti, Time of flight in perspective: instrumental and computational aspects of time resolution in positron emission tomography, IEEE Trans Radiat Plasma Med Sci 5 (5) (2021) 598–618.
[7] P. Lecoq, Pushing the limits in time-of-flight PET imaging, IEEE Trans Radiat Plasma Med Sci. 1 (2017) 473–485.
[8] Biograph Vision PET/CT 2019 usa.healthcare.siemens.com/molecular-imaging/pet-ct/biograph-vision.
[9] Philips Vereos PET/CT 2019 usa.philips.com/healthcare/product/HC882446/vereos-digital-petct-provenaccuracy-inspires-confidence#galleryTab=360.

[10] A. LaBella, S. Tavernier, C. Woody, et al., Toward 100 ps coincidence time resolution using multiple timestamps in depth-encoding PET modules: a Monte Carlo simulation study, IEEE Trans Radiat Plasma Med Sci. 5 (5) (2021) 679–686.
[11] A. Gonzalez-Montoro, M.N. Ullah, C.S. Levin, Advances in detector instrumentation for PET, J. Nucl. Med. 63 (8) (2022) 1138–1144.
[12] F. Pagano, N. Kratochwil, M. Salomoni, Advances in heterostructured scintillators: toward a new generation of detectors for TOF-PET, Phys. Med. Biol. 67 (2022) 135010.
[13] S. Gundacker, R.M. Turtos, E. Auffray, et al., High-frequency SiPM readout advances measured coincidence time resolution limits in TOF-PET, Phys. Med. Biol. 64 (5) (2019) 1361–6560.
[14] P. Cherenkov, Visible emission of clean liquids by action of γ radiation, Dokl. Akad. Nauk SSSR 451 (1934).
[15] J.V. Jelley, Cerenkov radiation and its applications, Br. J. Appl. Phys. 6 (1955) 227.
[16] S.E. Brunner, L. Gruber, J. Marton, et al., Studies on the Cherenkov effect for improved time resolution of TOF-PET, IEEE Trans. Nucl. Sci. 61 (2014) 443–447.
[17] N. Kratochwil, E. Auffray, S. Gundacker, Exploring Cherenkov emission of BGO for TOF-PET, IEEE Trans Radiat Plasma Med Sci. 5 (5) (2020) 619–629.
[18] S.E. Brunner, D.R. Schaart, BGO as a hybrid scintillator/Cherenkov radiator for cost effective time-of-flight PET, Phys. Med. Biol. 62 (2017) 4421–4439.
[19] S. Gundacker, R.M. Turtos, N. Kratochwil, et al., Experimental time resolution limits of modern SiPMs and TOF-PET detectors exploring different scintillators and Cherenkov emission, Phys. Med. Biol. 65 (2020) 025001.
[20] J.W. Cates, C.S. Levin, Electronics method to advance the coincidence time resolution with bismut germanate, Phys. Med. Biol. 64 (2019) 175016.
[21] N. Kratochwil, S. Gundacker, P. Lecoq, E. Auffray, Pushing Cherenkov PET with BGO via coincidence time resolution classification and correction, Phys. Med. Biol. 65 (2020) 115004.
[22] A. Gola, F. Acerbi, M. Capasso, et al., NUV-sensitive silicon photomultiplier technologies developed at Fondazione Bruno kessler, Sensors 19 (2) (2019) 308.
[23] C. Piemonte, F. Acerbi, A. Ferri, et al., Performance of NUV-hd silicon photomultiplier technology, IEEE Trans. Electron. Dev. 63 (2016) 1111–1116.
[24] S. Gundacker, Time Resolution in Scintillator Based Detectors for Positron Emission Tomography [Dissertation, Technische Universität Wien], reposiTUm, 2014, https://doi.org/10.34726/hss.2014.21431.
[25] S. Gundacker, A. Heering, The silicon photomultiplier: fundamentals and applications of a modern solid-state photon detector, Phys. Med. Biol. 65 (17) (2020) 17TR01.
[26] J.W. Cates, S. Gundacker, E. Auffray, et al., Improved single photon time resolution for analog SiPMs with front end readout that reduces influence of electronic noise, Phys. Med. Biol. 63 (2018) 185022.
[27] E. Roncali, S.I.I. Kwon, S. Jan, et al., Cerenkov light transport in scintillation crystals explained: realistic simulation with GATE, Biomed, Phys. Eng. Express 5 (2019) 035033.
[28] A. Gola, Silicon Photomultiplier technologies developed at FBK: roadmap towards 3D integrated devices at CERN Seminars 40/S2-D01. https://indico.cern.ch/event/1268951/, 2023.
[29] S. Gundacker, E. Auffray, P. Jarron, et al., On the comparison of analog and digital SiPM readout in terms of expected timing performance, Nucl. Instrum. Methods Phys. Res. A 787 (2014) 6–11.
[30] I. Kwon, T. Kang, M.K. Hammig, Experimental validation of charge-sensitive amplifier configuration that compensates for detector capacitance, IEEE Trans. Nucl. Sci. 63 (2016) 1202–1208.
[31] N. Zhang, M.J. Schmand, Bootstrapping Readout for Large Terminal Capacitance Analog-SiPM Based Time-Of-Flight PET Detector, US Patent, 2016. US2016/0327657.
[32] A. Gonzalez-Montoro, S. Pourashraf, J.W. Cates, C.S. Levin, Cherenkov radiation–based coincidence time resolution measurements in BGO scintillators, Front. Physiol. 10 (2022) 816384.
[33] J.Y. Yeom, R. Vinke, C.S. Levin, Side readout of long scintillation crystal elements with digital SiPM for TOF-DOI PET, Med. Phys. 41 (2014) 12250.
[34] F. Acerbi, G. Paternoster, S. Merzi, et al., NUV and VUV sensitive Silicon Photomultipliers technologies optimized for operation at cryogenic temperatures, Nucl. Instrum. Methods Phys. Res. A 1046 (2023) 167683.
[35] M. Capasso, et al., FBK VUV-sensitive Silicon Photomultipliers for cryogenic temperatures, Nucl. Instrum. Methods Phys. Res. A 982 (2020) 164478.
[36] Broadcom® AFBR-S4N33C013 NUV-HD Single Silicon Photomultiplier Data Sheet: https://docs.broadcom.com/doc/AFBR-S4N33C013-DS.
[37] A. Gola, C. Piemonte, A. Tarolli, Analog circuit for timing measurements with large area SiPMs coupled to LYSO crystals, IEEE Trans. Nucl. Sci. 60 (2) (2013) 1296–1302.
[38] A.E. Spinelli, F. Boschi, Novel biomedical applications of Cerenkov radiation and radioluminescence imaging, Phys. Med. 31 (2) (2015) 120–129.
[39] Saint-Gobain, BC-630 silicone grease DATASHEET from. https://www.crystals.saint-gobain.com/sites/imdf.crystals.com/files/documents/bc-630.pdf, 2017.
[40] C. Trigila, et al., The accuracy of Cerenkov photons simulation in geant4/gate depends on the parameterization of primary electron propagation, Front. Physiol. 10 (2022) 891602.
[41] P.A. Williams, A.H. Rose, K.S. Lee, et al., Optical, thermo-optic, electro-optic, and photoelastic properties of bismuth germanate (Bi4Ge3O12), Appl. Opt. 35 (1996) 3562–3569.
[42] A. Sanchez Gonzalez-Montoro, F. Majewski, S. at al, Highly improved operation of monolithic BGO-PET blocks, J. Inst. Met. 12 (2017). C11027.
[43] Trigila, C. Roncali, E. Effect of crystal-photodetector interface extraction efficiency on Cerenkov photons' detection time. Front. Physiol. 10: 2296-424X.
[44] J.W. Cates, W.S. Choong, Low power implementation of high frequency SiPM readout for Cherenkov and scintillation detectors in TOF-PET, Phys. Med. Biol. 67 (2022) 195009.
[45] R. Latella, A. Gonzalez, D. Bonifacio, et al., Exploiting Cherenkov radiation with BGO-based metascintillators, TechRxiv. Preprint (2022), https://doi.org/10.36227/techrxiv.21388863.v1.
[46] A. Gonzalez-Montoro, S. Pourashraf, J.W. Cates, C.S. Levin, Study of optical reflectors for a 100ps coincidence time resolution TOF-PET detector design, Biomed Phys Eng Express 15 (7) (2021), https://doi.org/10.1088/2057-1976/ac240e, 6.
[47] Analog Devices, AD8000 High Speed Operational Amplifier Data Sheet https://www.analog.com/media/en/technical-documentation/data-sheets/AD8000.pdf.
[48] MACOM MABA-007159 Data Sheet 2019 Cdn.macom.com/datasheets/MABA-007159-000000.pdf.
[49] Minicircuits MAR-6 RF Amplifier Data Sheet 2019 Minicircuits.com/pdfs/MAR-6+.pdf.
[50] I. Kwon, T. Kang, B.T. Wells, et al., Compensation of the detector capacitance presented to charge-sensitive preamplifiers using the Miller effect, Nucl. Instrum. Methods 784 (2015) 220–225.
[51] R. Vinke, S. Seifert, D.R. Schaart, et al., Optimization of digital time pickoff methods for LaBr3-SiPM TOF-PET detectors, NSS/MIC. IEEE Nuclear Science Symp. Conf. Record (Orlando), 2009, pp. 2962–2968.
[52] S. Seifert, D.R. Schaart, Improving the time resolution of TOF-PET detectors by double-side readout, IEEE Trans. Nucl. Sci. 62 (2015) 3–11.
[53] S. Gundacker, F. Acerbi, E. Auffray, et al., A State of the art timing in TOF-PET detectors with LuAG, GAGG and L(Y)SO scintillators of various sizes coupled to FBK-SiPMs, J. Instrum. 11 (2016).
[54] E. Berg, E. Roncali, S.R. Cherry, Optimizing light transport in scintillation crystals for time-of-flight PET: an experimental and optical Monte Carlo simulation study Biomed, Opt Express 6 (2015) 2220–2230.
[55] J. Maebe, S. Vandenberghe, Effect of detector geometry and surface finish on Cerenkov based time estimation in monolithic BGO detectors, Phys. Med. Biol. 5 (2) (2023) 68.
[56] Broadcom® AFBR-S4N44P164M 4×4 NUV-MT Silicon Photomultiplier Array Data Sheet: https://docs.broadcom.com/doc/AFBR-S4N44P164M-DS-4x4-NUV-MT-Silicon-Photo-Multiplier-Array.
[57] G. Ambrosi, et al., SiPM and Front-End Electronics Development for Cherenkov Light Detection, 2015 arXiv:1509.03207vol. 1.
[58] Hamamatsu Photonics, MPPC® S13360 Data sheet, https://www.hamamatsu.com/content/dam/hamamatsu-photonics/sites/documents/99_SALES_LIBRARY/ssd/s13360-2050ve_etc_kapd1053e.pdf.
[59] Hamamatsu Photonics, MPPC® S13370 Data sheet, https://hamamatsu.su/files/uploads/pdf/3_mppc/s13370_vuv4-mppc_b_(1).pdf.
[60] R. Álvarez-Garrote, et al., Measurement of the photon detection efficiency of Hamamatsu VUV4 SiPMS at cryogenic temperature, Nucl. Instrum. Methods 1064 (2024) 169347.
[61] Hamamatsu Photonics, MPPC® S14160 and S14161 Data sheet, https://www.hamamatsu.com/content/dam/hamamatsu-photonics/sites/documents/99_SALES_LIBRARY/ssd/s14160_s14161_series_kapd1064e.pdf.
[62] S. Gundacker, et al., On timing-optimized SiPMs for Cherenkov detection to boost low cost time-of-flight PET, Phys. Med. Biol. 68 (2020) 165016.
[63] J. Du, Performance of dual-ended readout PET detectors based on BGO arrays and BaSO4 reflector, IEEE Trans Radiat Plasma Med Sci. 12 (6) (2021) 522–528, 5.
[64] G. Konstantinou, P. Lecoq, J.M. Benlloch, A.J. Gonzalez, Metascintillators for ultrafast gamma detectors: a review of current state and future perspectives, IEEE Trans Radiat Plasma Med Sci. 6 (1) (2022).
[65] R.M. Turtos, S. Gundacker, E. Auffray, P. Lecoq, Towards a metamaterial approach for fast timing in PET: experimental proof-of-concept, Phys. Med. Biol. 64 (2019) 18.
[66] R. Pestotnik, Use of Cherenkov light in TOF-PET, Jozef Stefan Institute - Ljubljana, Slovenia IL NUOVO CIMENTO 43 C (2020) 18, https://doi.org/10.1393/ncc/i2020-20018-3.